^{9}Be(p,pα)^{5}He cluster knockout reaction with 150 MeV polarized protons

C. W. Wang,* P. G. Roos, N. S. Chant, G. Ciangaru,† F. Khazaie, and D. J. Mack
Department of Physics and Astronomy, University of Maryland, College Park, Maryland 20742

A. Nadasen
Department of Natural Sciences, University of Michigan-Dearborn, Dearborn, Michigan 48128

S. J. Mills
Council of Scientific and Industrial Research, Faure, South Africa

R. E. Warner
Oberlin College, Oberlin, Ohio 44074

E. Norbeck
Department of Physics and Astronomy, University of Iowa, Iowa City, Iowa 52242

F. D. Becchetti, J. W. Janecke, and P. M. Lister
Department of Physics, University of Michigan, Ann Arbor, Michigan 48109
(Received 7 December 1984)

The (p,pα) cluster knockout reaction on ^{9}Be was investigated using polarized incident protons. Coincident data for eight quasifree angle pairs were obtained at a bombarding energy of 150 MeV. Both differential cross sections and analyzing powers were measured for the energy-sharing distribution. Distorted wave impulse approximation calculations indicate that the reaction is dominated by a quasifree knockout process, and that a *D*-state component of the cluster-core wave function is important for larger momentum transfer. Extracted absolute spectroscopic factors for both *S*- and *D*-state knockout are in good agreement with theoretical predictions. The analyzing power follows the trend of free p-^{4}He scattering and agrees with the distorted wave impulse approximation calculation reasonably well. Near zero recoil momentum, the spin-orbit interaction in the distorted waves plays little role.

I. INTRODUCTION

Quasifree alpha-cluster knockout reactions on light- and medium-mass nuclei have been investigated by several authors[1–7] over the past ten years. For bombarding energies in excess of 100 MeV the (p,pα) reaction appears to be a reliable tool for determining absolute alpha-particle spectroscopic factors. On the other hand, nuclear structure information derived from the (α,2α) reaction is more uncertain. This appears to be due either to significant contributions from more complicated reaction mechanisms or to effects arising from strong absorption which limits the yield to the extremely low density region of the nucleus. Typically, quasifree cluster-knockout reactions are most sensitive to the low momentum components of the cluster-core wave function and thus complement cluster-transfer reactions[8–11] which are most sensitive to relatively high-momentum components of the cluster-core wave function. The complementarity of the two types of reactions was demonstrated by Carey *et al.*[1] for the (p,pα) and (^{6}Li,d) ground state transitions. However, the knockout reaction offers better hope for the determination of absolute spectroscopic factors.

In the analysis of the quasifree cluster-knockout reaction one generally uses a factorized distorted-wave impulse approximation (DWIA).[12–14] Neglecting spin-orbit terms in the proton-nucleus optical potential, the expression for the differential cross section is essentially a product of the half-off-shell cross section for the projectile-cluster interaction and a distorted momentum distribution for the cluster-core relative motion. The inclusion of distortions removes most of the limitations of plane-wave impulse approximation (PWIA) calculations. These include an excessively large predicted absolute cross section and the prediction of deep minima arising from nodes in the cluster-core wave function which are not seen experimentally. The removal of the minima by the averaging produced from the distribution of momenta present in the distorted waves allows one to predict properly the width of the experimental momentum distribution.

Presently, DWIA calculations appear to provide a rather good description of the available (p,pα) data. However, the reliability of quantitative nuclear-structure information extracted from these data depends upon the adequacy of our treatment of the reaction dynamics. Several tests of the DWIA description of the (p,pα) reaction have been made.[2,15] One of the most sensitive is a test of the factorization approximation by comparing angular distributions for the (p,pα) reaction with those for free p-α scattering. At 100 MeV (Ref. 2) the factorization approximation was found to be reasonably good, although over an extended angular range discrepancies of as much as a factor of 2 were observed.

With the availability of intense beams of medium-

energy polarized protons, more detailed tests of the DWIA description of (p,pα) reactions become possible. For example, measurements of (p,pα) analyzing powers can be compared to analyzing powers measured in free p-α scattering. In the simplest DWIA treatment, these two quantities should be identical. In practice, since the relative phase of different t-matrix elements is involved, considerable sensitivity to details of the reaction description can be expected.

The only published measurements of (p,pα) analyzing powers are for the ^{6}Li(p,pα)d reaction[16] at 40 MeV. To provide further tests of the adequacy of the DWIA treatment of medium-energy (p,pα) reactions, including their spin dependence, we have measured cross sections and analyzing powers for the ^{9}Be(p,pα)^{5}He reaction at 150 MeV. The experimental details are given in Sec. II. The ^{9}Be nucleus is a good candidate for the present study since the ^{9}Be(p,pα) reaction has been previously studied in detail with unpolarized protons at 100 MeV.[2,3] This work gives roughly equal $L=0$ and 2 spectroscopic factors of approximately 0.5 in agreement with the predictions of Kurath.[17] The experimental cross section and analyzing power data are presented in Sec. III.

Since measurements of analyzing powers are made, we have included spin-orbit distortions in the DWIA calculations. As a result the two-body p-α cross section and analyzing power do not enter as multiplicative factors. Rather, one must incorporate a detailed description of the half-shell t-matrix elements. In the DWIA analysis presented in Sec. IV we have generated t-matrix elements using an optical-model description of the p-α interaction. The present work is summarized in Sec. V.

II. EXPERIMENT

The experiment was carried out at the Indiana University Cyclotron Facility. A 150.5 MeV polarized proton beam with polarization between 0.75 and 0.77 normal to the scattering plane was used to bombard a ^{9}Be target at the center of a 160 cm diam scattering chamber. The intensity of the beam varied from 5 to 25 nA depending on the angle setting of the experiment. The intensity and location of the beam were monitored with a split Faraday cup.

Two detector telescopes were used to detect the outgoing particles produced by the ^{9}Be(p,pα)^{5}He reaction. A telescope consisting of a 1000 μm silicon surface-barrier detector followed by a sodium iodide scintillation detector was used for proton detection. A 150 μm silicon surface-barrier ΔE-detector and a 5 mm Si(Li) E-detector formed another telescope for alpha detection. The two telescopes were mounted coplanar with and on opposite sides of the incident beam. Slits with circular apertures were used to define a solid angle of 6.78$\pm$0.02 msr for the proton telescope and of 4.52$\pm$0.05 msr for the alpha telescope. The angular separation between these two telescopes was calibrated by using a coincident measurement of p-d scattering on a CD_2 target.

Besides the 2.5 mg cm^{-2} thick ^{9}Be target, a 3.1 mg cm^{-2} CH_2 target, a 3.32 mg cm^{-2} CD_2 target, and a blank target were mounted on a target ladder. These additional targets enabled us to perform energy calibrations and background measurements.

The electronics used for signal processing were standard. The outputs of all solid state detectors were sent to charge-sensitive preamplifiers. The output of the NaI detector was taken from the fifth dynode and sent to an emitter follower. Slow linear signals, properly amplified and delayed, were digitized by analog-to-digital converters (ADC) interfaced to a Harris computer. A fast signal from each detector was also extracted to generate gating signals. The fast logic signals from the two telescopes were used to start and stop a time-to-digital converter (TDC), with a time range corresponding to several beam bursts. This allowed simultaneous measurement of real and accidental coincidences. A pulser signal sent to each preamplifier and processed together with the real data was used to correct for electronic dead-time losses.

The ADC pulse-height information for each detector, together with the TDC output and bit registers, were written event by event on magnetic tapes. The outputs of a number of scalers, including the current integrator, were also written on the event tape. A variety of one- and two-dimensional histograms were generated by software during the experiment. Visual displays of these histograms were used to monitor the detector gain, particle identification (PID), and the statistics for the different coincident events. At the end of each run, the histograms and scalers were dumped to another magnetic tape.

Coincident data were taken for eight angle pairs in which the angle of the proton arm ranged from 25° to 90°. The angle settings are listed in Table I. The angles of the alpha arm were chosen such that zero recoil momentum of the residual ^{5}He nucleus was kinematically allowed. Results for other possible three-body reactions were also recorded. As a continuous monitor of gain, singles events for both telescopes were recorded, prescaled by a factor of $\frac{1}{10}$ to $\frac{1}{1000}$ according to the angle of the telescope.

For the $\theta_p=25°$ and 30° runs, a ΔE-E coincidence for the alpha telescope was not required, since most of the α particles from the quasifree knockout reaction were stopped in the ΔE detector. For the $\theta_p=40°$ runs, we took data with and without the ΔE-E alpha coincidence requirement. For $\theta_p=80°$ and 90°, we tilted the normal of the target by 10° and 36°, respectively, from the beam

TABLE I. Angle pairs, cross sections, and analyzing powers at quasifree peaks.

θ_p/θ_α	$\theta_{p\text{-}\alpha}$[a] (c.m.)	$d^3\sigma/d\Omega^2dE$ p[b] (μb/sr^2 MeV)	A_y[b]
25°/−72.8°	31.9	355 ±15	0.84±0.03
30°/−69.8°	38.2	408 ±14	0.57±0.03
40°/−63.9°	50.5	169 ± 6.8	−0.04±0.04
50°/−58.1°	62.5	86.7 ± 3.1	−0.45±0.03
60°/−52.4°	74.1	45.3 ± 2.2	−0.79±0.04
70°/−46.9°	85.3	17.9 ± 0.7	−0.77±0.03
80°/−41.6°	95.9	9.84± 0.65	−0.33±0.06
90°/−36.6°	106.1	6.57± 0.37	0.21±0.05

[a]Calculated for zero recoil momentum point.
[b]Errors reflect counting statistics only.

direction to the proton side in order to reduce the energy loss for the outgoing protons in the target.

III. EXPERIMENTAL RESULTS

Off-line analysis of the event-by-event data was carried out using the program LISA running on the VAX 11/750 computer of the University of Maryland Experimental Nuclear Physics Group. The ΔE_p vs E_p and ΔE_α vs E_α two-dimensional displays were linearized and projected onto the particle identification axes. Events corresponding to different masses were well separated for both charge-one and charge-two telescopes, which guaranteed the separation of different reaction products during the data reduction. Two-dimensional spectra of T_p+T_α vs T_p ($T_p=\Delta E_p+E_p$, $T_\alpha=\Delta E_\alpha+E_\alpha$) were generated for each data run. The events along the three-body kinematic locus were linearized and projected onto $T_p+T_\alpha+T_R$ where T_R is the calculated recoil energy of the residual nucleus. Using a gate corresponding to the specific reaction Q value, events were then selected and projected onto T_p, the proton energy axis, to create "PALPHA histograms." These energy-sharing spectra, gated by the coincidence requirement, particle identification, and spin state of the incoming protons, with random events subtracted and dead-time losses corrected, were used for calculations of the (p,pα) cross section and analyzing power.

The cross sections (corrected for distortion effects) and analyzing powers of the ^{9}Be(p,pα) knockout reaction at the quasifree peak (zero recoil momentum) of each data set are plotted in Figs. 1 and 2 as a function of the center-of-mass scattering angle ($\theta_{c.m.}$) in the proton-alpha rest frame. It is expected that, if the quasifree-knockout reaction mechanism is a good approximation at the energy studied, these cross sections and analyzing powers should be nearly the same as in p-^{4}He elastic scattering at an appropriate energy (in our case, we have assumed this energy to be 148 MeV, the total kinetic energy in the emitted p-α rest frame which corresponds to the so-called final-energy prescription). Due to the distortion effects it is necessary to correct the cross-section data using distorted-wave calculations as discussed in Sec. IV. In the case of analyzing powers, distortions have little effect. Comparing with the p-^{4}He results of Cormack *et al.*[18] at $E=147$ MeV, we see that the corrected cross sections are very nearly the same. For the analyzing powers both sets of data have the same oscillatory pattern in the angular range covered by the experiments. The phase of the oscillation is nearly identical for the two results. However, the peak analyzing powers for (p,pα) are about 13% smaller for $\theta_{c.m.}<90°$. Recent analyzing power measurements of p-^{4}He scattering at $E=150$ MeV (Ref. 19) give $A=0.610\pm0.006$ at $\theta_{c.m.}=38°$, which is about 15% smaller than the result of Ref. 18. Our result at this angle is consistent with these new measurements within experimental error. The results of the analyzing power obtained from the quasifree peaks are listed in Table I.

The distribution of the analyzing power as a function of outgoing proton energy was also extracted for each data set. The results are plotted in the lower panels of Figs. 3—10. A small arrow in each plot indicates the position

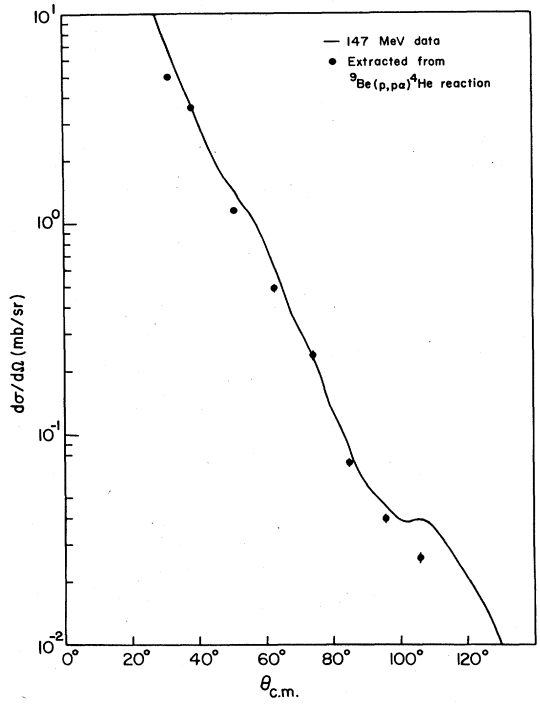

FIG. 1. ^{9}Be(p,pα)^{5}He cross sections for the quasifree peak (zero recoil momentum) as a function of the two-body p-α c.m. scattering angle. The data have been corrected for the variation in distortions using DWIA calculations and normalized to free p-α scattering. The curve represents the 147 MeV p-α elastic scattering data of Ref. 18.

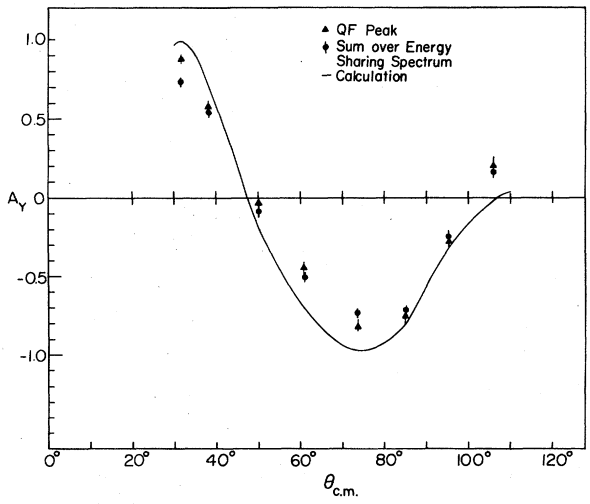

FIG. 2. ^{9}Be(p,pα)^{5}He analyzing power measurements corresponding to the cross section measurements presented in Fig. 1. The symbols correspond to the following: triangles, A_y at the quasifree peak; points, A_y summed over the full energy sharing distribution. The curve represents the free p-α data of Ref. 18.

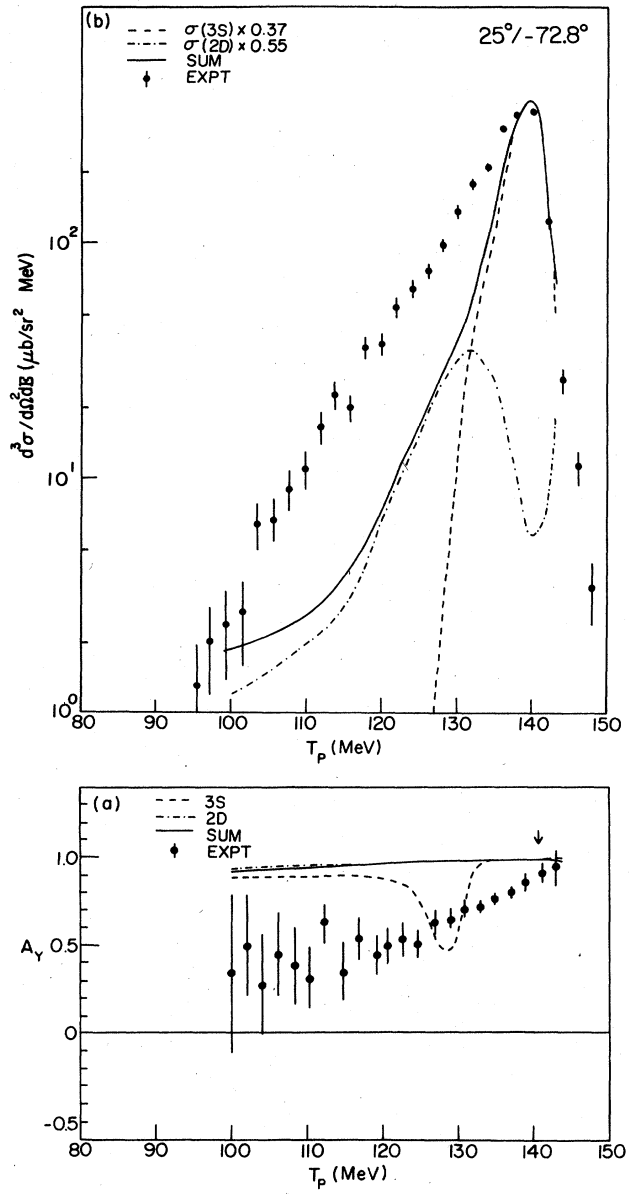

FIG. 3. Energy sharing cross section and analyzing power distributions for ^{9}Be(p,pα)^{5}He at $\theta_p/\theta_\alpha = 25°/-72.8°$. The curves correspond to DWIA calculations for $L=0$ and 2 knockout and their sum normalized as indicated.

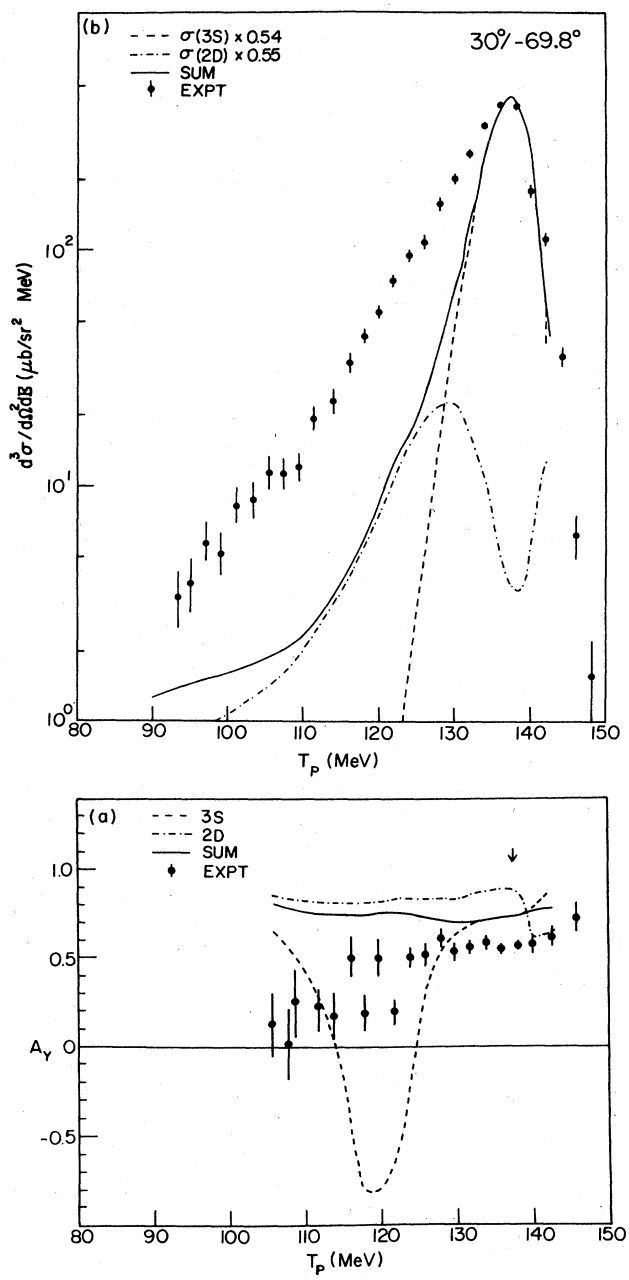

FIG. 4. Energy sharing cross section and analyzing power distributions for ^{9}Be(p,pα)^{5}He at $\theta_p/\theta_\alpha = 30°/-69.8°$. The curves correspond to DWIA calculations for $L=0$ and 2 knockout and their sum normalized as indicated.

of the quasifree peak. The error bars on each data point reflect statistical errors only. In general the data do not show dramatic changes with detected-particle energy. In some cases distributions are fairly flat, for example for $\theta_p = 40°$, 50°, 60°, and 70°. In other cases, for example $\theta_p = 25°$, 30°, and 80°, the distributions show a smooth decrease from large values (of 0.6 to 0.9) at around $T_p = 140$ MeV to more modest values at lower energies.

The energy-sharing cross-section distributions are shown in the top panels of Figs. 3—10. With the exception of $\theta_p = 40°$, all of these spectra show a smooth prominent peak around $p_3 = 0$, where p_3 is the recoil momentum of the residual nucleus. In the $\theta_p = 40°$ spectrum additional peaks show up on the high proton-energy side of the quasifree peak. These contributions are also observed in other (p,pα) knockout reactions[2,4] and come from alpha emission following the target excitation to excited states at ~ 8 MeV excitation or less. The reason that these sequential decays are not observed in the $\theta_p = 25°$ and 30° spectra is that the target thickness seen from the alpha

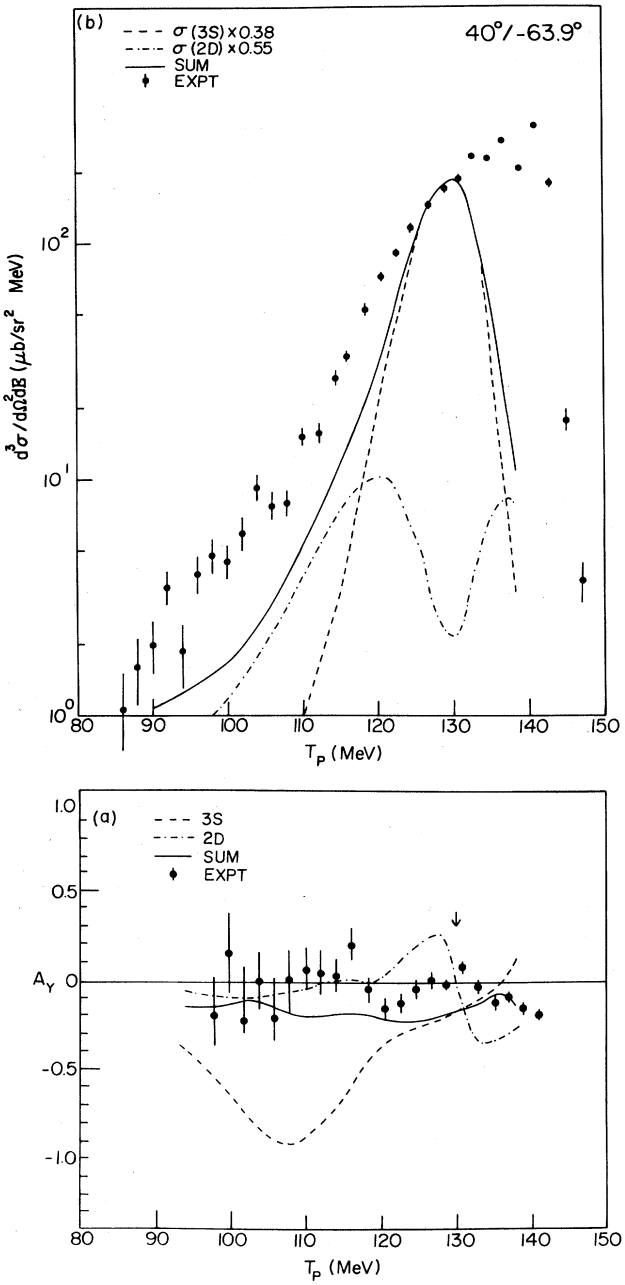

FIG. 5. Energy sharing cross section and analyzing power distributions for ^{9}Be(p,pα)^{5}He at $\theta_p/\theta_\alpha = 40°/-63.9°$. The curves correspond to DWIA calculations for $L=0$ and 2 knockout and their sum normalized as indicated.

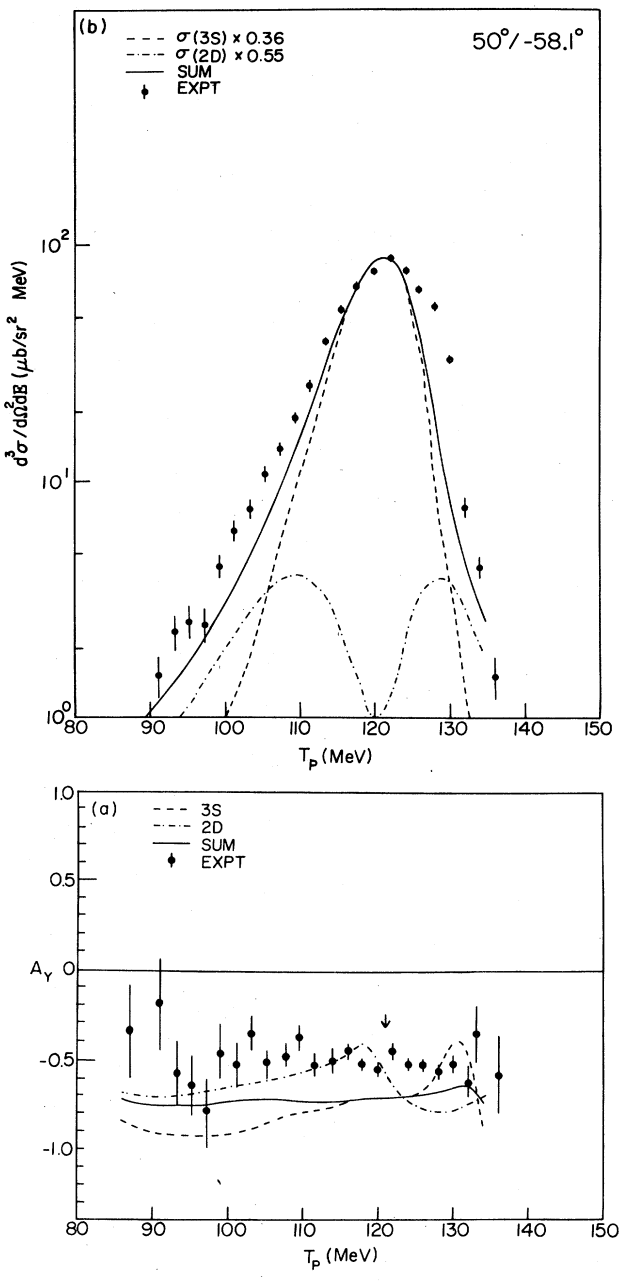

FIG. 6. Energy sharing cross section and analyzing power distributions for ^{9}Be(p,pα)^{5}He at $\theta_p/\theta_\alpha = 50°/-58.1°$. The curves correspond to DWIA calculations for $L=0$ and 2 knockout and their sum normalized as indicated.

arm for these two angular sets exceeds the range of the corresponding α particles. In addition, it is estimated that the quasifree peak height of the $\theta_p=25°$ spectrum is suppressed by about 12% due to target thickness effects, which in part compensates for the slight discrepancy at forward angles in the factorization test shown in Fig. 1.

Of all these energy sharing distributions the $\theta_p=50°$ and 60° spectra give the most symmetric distribution with respect to $p_3=0$, except for a rather prominent shoulder at around $T_p=125$ and 120 MeV, respectively. This shoulder also shows up in the $\theta_p=80°$ and 90° spectra at a proton energy about 10 MeV higher than that of the quasifree peak. The full width at half maximum of the 50° and 60° distributions with respect to p_3 is measured to be about 55 MeV/c on the low T_p side of the quasifree peak ($p_3=0$) and about 70 MeV/c on the high T_p side in-

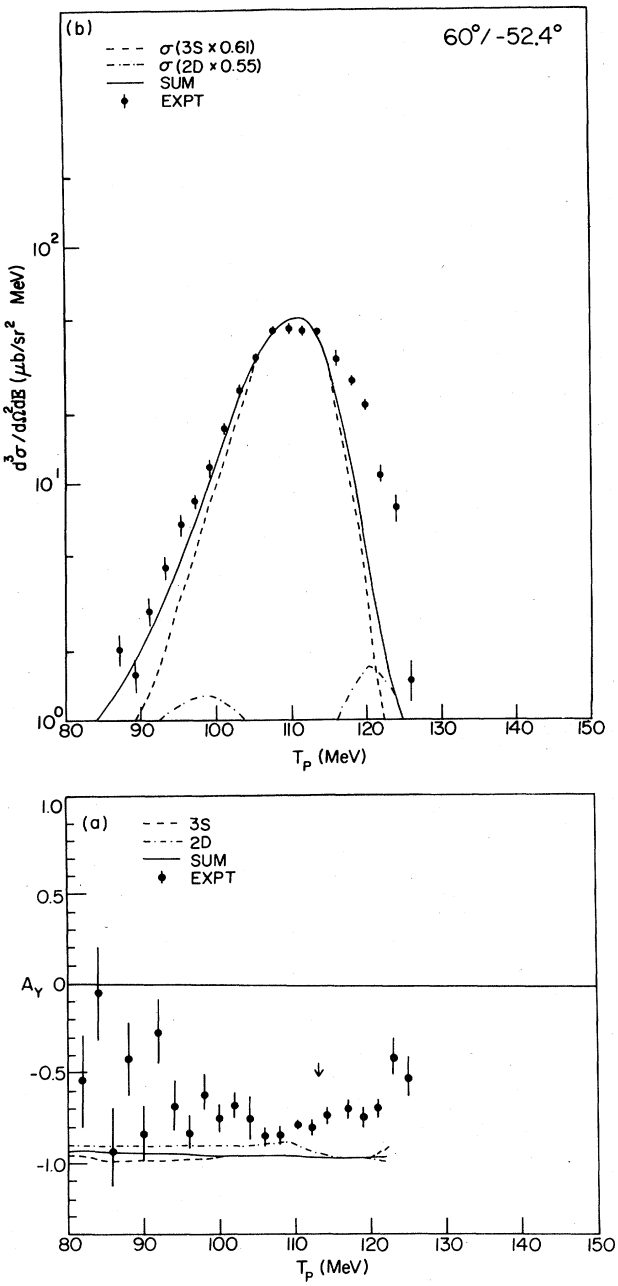

FIG. 7. Energy sharing cross section and analyzing power distributions for ^{9}Be(p,pα)^{5}He at $\theta_p/\theta_\alpha = 60°/-52.4°$. The curves correspond to DWIA calculations for $L=0$ and 2 knockout and their sum normalized as indicated.

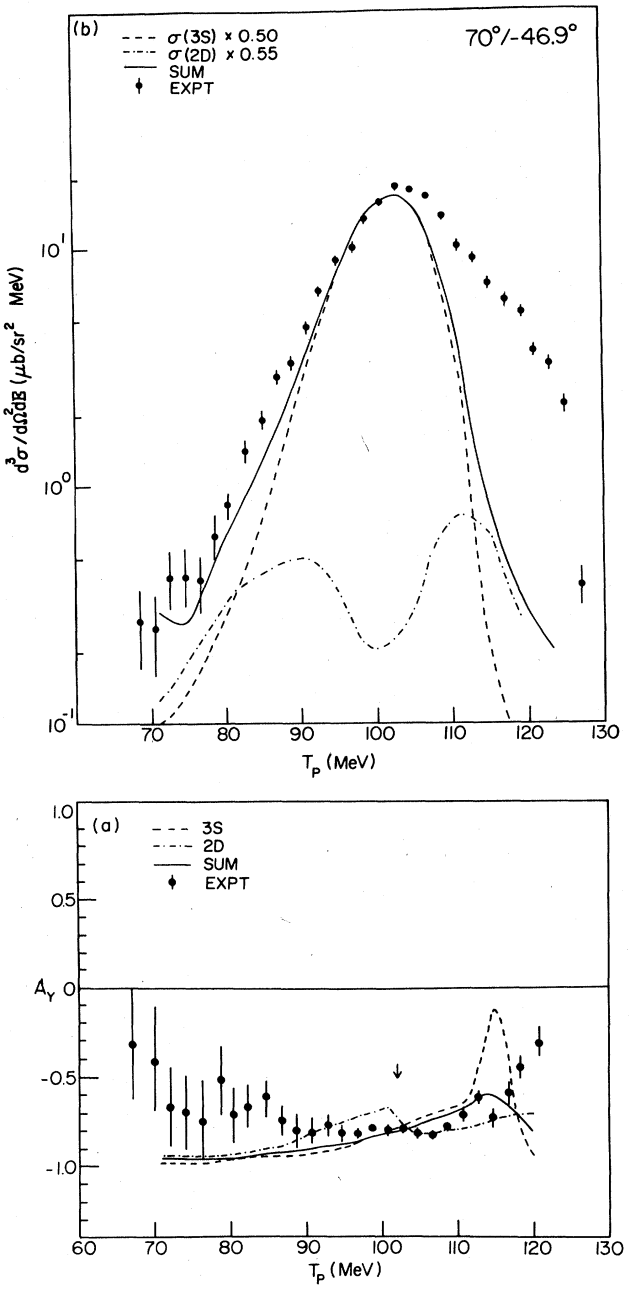

FIG. 8. Energy sharing cross section and analyzing power distributions for ^{9}Be(p,pα)^{5}He at $\theta_p/\theta_\alpha = 70°/-46.9°$. The curves correspond to DWIA calculations for $L=0$ and 2 knockout and their sum normalized as indicated.

cluding the contribution of the shoulder. This width is just the width of the distorted momentum distribution of the

$$^{4}\text{He(g.s.)} + ^{5}\text{He(g.s.)}$$

in the ^{9}Be(g.s.) target. In the plane wave limit, it is the momentum distribution of alpha particles in ^{9}Be. As shown by the distorted wave impulse approximation (DWIA) calculations,[14] the distorted momentum distribution differs from the true momentum distribution mainly in absolute magnitude and the removal of the deep minima predicted by PWIA. The DWIA distribution is somewhat broader than that of the PWIA, but both distributions are highly symmetric and the widths remain about the same for all angular sets if the distortion is not too severe. Thus it appears that the "shoulders" in the spectra arise from contributions from reactions other than quasifree knockout which are kinematically indistinguishable. One of the candidates for this contribution is the

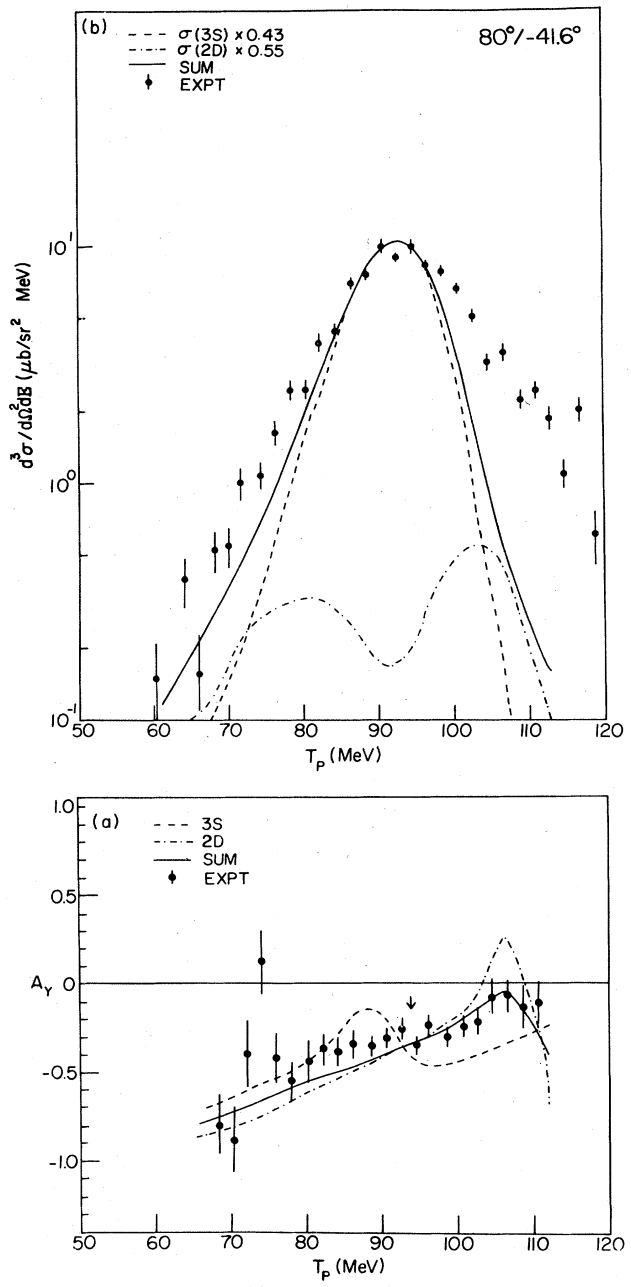

FIG. 9. Energy sharing cross section and analyzing power distributions for ^{9}Be(p,pα)^{5}He at $\theta_p/\theta_\alpha = 80°/-41.6°$. The curves correspond to DWIA calculations for $L=0$ and 2 knockout and their sum normalized as indicated.

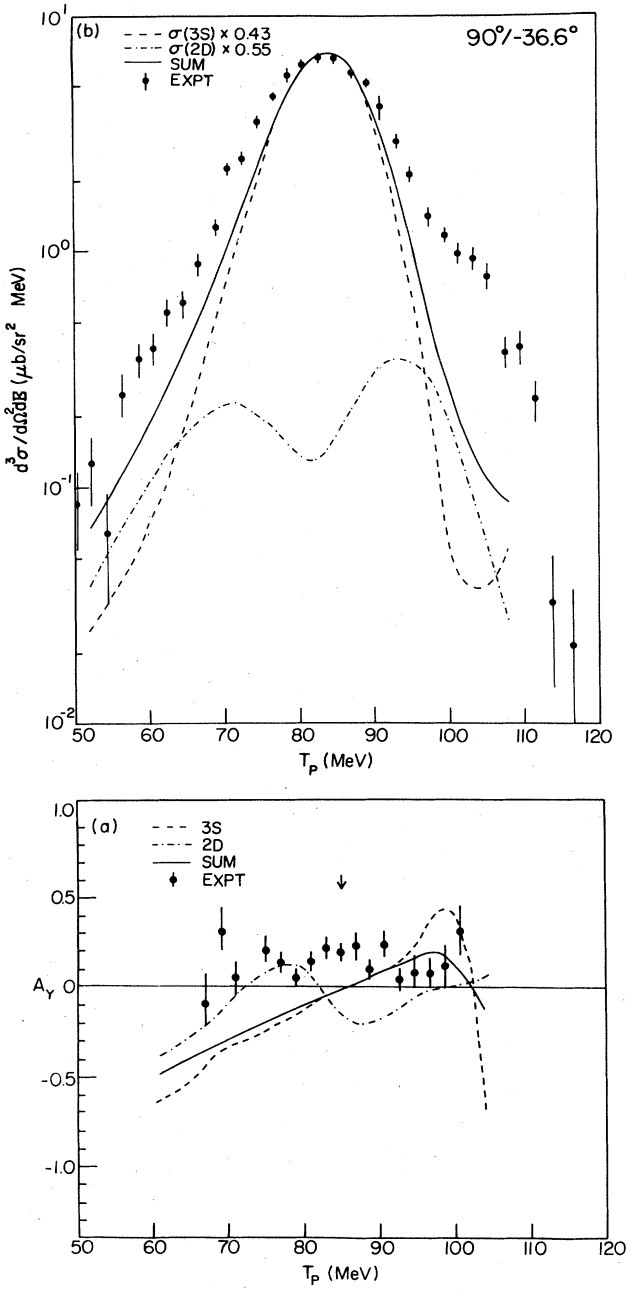

FIG. 10. Energy sharing cross section and analyzing power distributions for ^{9}Be(p,pα)^{5}He at $\theta_p/\theta_\alpha = 90°/-36.6°$. The curves correspond to DWIA calculations for $L=0$ and 2 knockout and their sum normalized as indicated.

sequential alpha decay following the excitation of the target nucleus ^{9}Be to an excitation energy of about 15 MeV where several broad excited states have been observed and have been reported in other (p,pα) studies.[4]

IV. DWIA ANALYSIS

The impulse approximation has proven to be quite satisfactory for knockout reactions at energies greater than 100 MeV.[2,4,6,15] Recent DWIA calculations[14] show that the spin-orbit interaction in the distorted waves can play an important role in the prediction of both the cross section and the analyzing power in (p,2p) and (p,pn) reactions. For the case that includes a spin-orbit interaction in the distorted waves, the differential cross section can never be factorized.[12] Following Ref. 14 the cross section for the reaction $A(a,cd)B$ can be reduced to the following expression:

$$\sigma_{BA}(\rho_a')=\frac{2\pi}{h\nu}\omega_B C^2S\sum_{\substack{\rho_c' \\ L\Lambda}}\left|\sum_{\rho_a\sigma_a\sigma_c\sigma_c'} D^{S_a}_{\rho_a\rho_a'}(R_{ap})D^{S_c^*}_{\sigma_c\sigma_c'}(R_{ac})T^{L\Lambda}_{\substack{\sigma_a\sigma_c' \\ \rho_a\rho_c'}}\langle\sigma_c\,|\,t\,|\,\sigma_a\rangle\right|^2, \tag{1}$$

for the case where particles b and d are spinless. The cross section is given for a specific value of ρ_a', the spin of the projectile. The D's are rotation matrices, $\langle\sigma_c\,|\,t\,|\,\sigma_a\rangle$ is the matrix element of the two-body p-α transition operator, and

$$T^{L\Lambda}_{\substack{\sigma_a\sigma_c' \\ \rho_a\rho_c'}}=(2L+1)^{-1/2}\int\chi^{(-)*}_{\sigma_c'\rho_c'}(\mathbf{r})\chi^{(-)*}_{\alpha}(\mathbf{r})\phi_{L\Lambda}(\mathbf{r})\chi^{(+)}_{\sigma_a\rho_a}(\gamma\mathbf{r})d\mathbf{r}\,, \tag{2}$$

with the χ's denoting the distorted waves and $\phi_{L\Lambda}$ the wave function of the cluster-core relative motion. More complete details of the notation are to be found in Ref. 14 including some details of the computer code THREEDEE used to carry out the calculations. The spectroscopic factor C^2S was set to unity in the calculation, and an experimental spectroscopic factor extracted by normalizing to the experimental data.

It is evident from Eq. (1) that, as a result of the inclusion of spin-orbit terms in the distorting potentials, the p-α cross section no longer appears as a multiplicative factor. Rather, the individual t-matrix elements must be calculated in a spin representation. At each angle this involves three independent real quantities which we have obtained from a p+^{4}He optical model potential fitted to experimental data. The potential was parametrized with a Woods-Saxon form including absorption, spin-orbit interaction, and exchange terms. The parameters are listed in Table II. With this potential, we are able to reproduce satisfactorily the 147 MeV p-^{4}He differential cross sections and analyzing power.[18] In the spirit of our factorized DWIA approximation the p-α t matrix is properly half-off-the-energy-shell. This effect was estimated for the present data with the Coulomb part of the p-α optical potential set to zero. In all cases the half-shell calculations were consistent to within 2% with calculations setting the p-α t matrix on shell at the emitted p-α rest-frame energy and with the Coulomb term included. The results of these latter calculations are shown herein. Clearly, in a more nearly correct analysis, the factorization approximation should be eliminated which would lead to the introduction of fully-off-shell t-matrix elements.

The distorted waves were generated using optical-model parameters fitted to elastic scattering data. These parameters are also listed in Table II. For the incoming channel we used a p+^{9}Be potential at 160 MeV.[20] For the p+^{5}He and α+^{5}He channels we used the same potentials as those for the 101 MeV ^{9}Be(p,pα) out-of-plane calculation.[4] The sensitivity of the differential cross sections to reasonable changes in the distorting potentials has been tested by several authors[2,4,6] who suggest an upper limit on the variation of about 25%. In our analysis we find somewhat less uncertainty at 150 MeV. In addition, the effect of reasonable changes in the distorting potentials on the analyzing powers was investigated at the peak of A_y, where it was found to be negligible.

The eigenfunction of a real Woods-Saxon well that reproduced the alpha separation energy was used for the alpha-core relative motion wave function. The geometry of the potential well was chosen to approximate an alpha-nucleus folding-model calculation.[2] The quantum numbers of the bound state-wave function were chosen on the basis of the conservation of shell-model oscillator quanta and of parity by assuming the configurations $(1s^4)(1p^5)$ for ^{9}Be(g.s.), $(1s^4)(1p^1)$ for ^{5}He(g.s.), and $(1s^4)$ for ^{4}He(g.s.). Since both ^{9}Be(g.s.) and ^{5}He(g.s.) have spin and parity $J^\pi=\frac{3}{2}^-$, both $3S$ and $2D$ cluster-core states are possible. Consequently, $3S$ and $2D$ calculations were carried out for all the data.

Shell-model calculations[17] and experimental results[4] indicate that the $3S$- and $2D$-component alpha spectroscopic factors are about equal for the ^{9}Be nucleus. DWIA calculations with equal spectroscopic factors give a ratio of the $3S$ to $2D$ cross section at the quasifree peak of 124/1 for the angle pair $\theta_p/\theta_\alpha=25°/-72.78°$, decreasing to 52/1 for 90°/−36.55°. Thus, it is quite safe to normalize the $3S$ contribution by comparing the calculated and ex-

TABLE II. Optical potential parameters.[a]

System	V_0	r_0	a_0	r_C	W_0	W_D	r_0'	a_0'	V_{so}	W_{so}	r_s	a_s	V_{ex}	r_{ex}	a_{ex}
p-^{9}Be	16.2	1.0	0.385	1.3	14	0	1.55	0.4	2.5	0	1.0	0.385			
p-^{5}He	37.8	1.14	0.79	1.32	0	4.5	1.32	0.44	6.0	−2	1.2	0.65			
α-^{5}He	88.9	0.99	0.81	1.2	4.9	0	3.01	0.58							
p-^{4}He	3.768	2.021	0.63	1.36	11.54	0	1.505	0.307	6.63	−3.2	0.85	0.23	−0.4	1.74	0.08
^{4}He-^{5}He	95.54	1.35	0.73	1.36											

[a]The optical potential is defined to be

$$-U(r)=\frac{V_0}{1+e^x}+\frac{iW_0}{1+e^{x'}}+\frac{4iW_De^{x'}}{(1+e^{x'})^2}+(-1)^l\frac{V_{ex}}{1+e^{x''}}+\left[\frac{h}{m_\pi c}\right]^2\mathbf{l}\cdot\boldsymbol{\sigma}\frac{1}{ra_s}\frac{(V_{so}+iW_{so})e^{x_s}}{(1+e^{x_s})^2}-U_{Coul}(R_C)\,,$$

where $x=(r-r_0A^{1/3})/a_s$, $x'=(r-r_0'A^{1/3})/a_0'$, $x''=(r-r_{ex}A^{1/3})/a_{ex}$, and $x_s=(r-r_sA^{1/3})/a_s$. U_{Coul} is the Coulomb potential of uniform charged sphere with $R_C=r_CA^{1/3}$. All energies are in units of MeV and lengths in fm.

TABLE III. Absolute α-spectroscopic factors for $^9Be \rightarrow \alpha + {}^5He$.

θ_p/θ_α	$S_\alpha(3S)$[a]	$\langle S_\alpha(3S)\rangle$	$S_\alpha(2D)$
25°/−72.8°	0.37±0.02		
30°/−68.8°	0.54±0.02		
40°/−63.9°	0.38±0.02		
50°/−58.1°	0.36±0.02	0.45	0.55
60°/−52.4°	0.61±0.03	(0.56)[b]	(0.55)[b]
70°/−46.9°	0.50±0.02		
80°/−41.6°	0.43±0.03		
90°/−36.6°	0.43±0.03		

[a]Errors reflect statistics.
[b]Reference 17.

perimental results at the quasifree peak. The extracted alpha spectroscopic factors for the $3S$ state from each angle pair is shown in Table III where the uncertainties reflect the counting statistics only. Averaging the results obtained at different angles yields 0.45 which is to be compared with the shell model prediction[17] of 0.56 and earlier (p,pα) studies[4] which yield 0.45. For the different angles the mean deviation is about 19% from the average value. This variation in the spectroscopic factor is an indication of a modest breakdown in the factorization approximation similar to that observed at 100 MeV.[2] However, the deviation is quite small. For the $L=2$ component the coplanar data do not very effectively determine the corresponding normalization. Thus we have chosen to follow the noncoplanar studies of Nadasen *et al.*[4] and the shell model calculations,[17] and used a spectroscopic factor of 0.55 for all calculations.

The analyzing powers obtained from the DWIA calculation at the quasifree peak are plotted in Fig. 2 along with the experimental results in the range $30° \leq \theta_{c.m.} \leq 110°$, where $\theta_{c.m.}$ is the two-body center-of-mass scattering angle in the emitted $p + {}^4He$ rest system. The calculated angular distribution is quite consistent with the shape and magnitude of the experimental data. It is worth noting that the analyzing powers calculated using the DWIA are essentially the same as those of the 147 MeV p-^{4}He elastic scattering. In order to examine the effect of distortions on the analyzing power, we set to zero the spin-orbit interaction in the proton distorted waves and repeated some calculations. On omitting spin-orbit terms the change in analyzing power is at most 0.02, a negligible change in comparing with the peak value of about 0.9. This result obviously differs from the (p,2p) and (p,pn) cases.[14]

The energy-sharing distributions of the analyzing powers versus the outgoing proton energies were also calculated. The differential cross sections for each spin state of the incoming proton were obtained for the $3S$ state, the $2D$ state, and the sum of the two states with the normalization factors specified earlier. The calculated analyzing powers for the individual angular momenta and sum are shown in Figs. 3—10. The $3S$ distribution shows a pronounced dip in analyzing power on the low T_p side of the quasifree peak at $p_3 \sim 130$ MeV/c for the angle pair $\theta_p/\theta_\alpha = 25°/-72.78°$ ($\theta_{c.m.} \sim 32°$). This location corresponds to a node in the $3S$ wave function. This dip becomes more prominent at $\theta_{c.m.} \sim 38°$ and then gradually disappears by $\theta_{c.m.} \sim 74°$. At larger angles a broad peak shows up on the high T_p side for $\theta_{c.m.} \geq 85°$, becoming more prominent as $\theta_{c.m.}$ increases. At $\theta_{c.m.} \sim 74°$ ($\theta_p/\theta_\alpha = 60°/-52.36°$) both the dip and the peak vanish giving rise to a flat distribution in analyzing power. Clearly the $3S$ contribution alone cannot reproduce the experimental results, except for one angle pair $\theta_p/\theta_\alpha = 60°/-52.36°$. The $2D$ calculation produces nearly a constant analyzing power for $\theta_{c.m.} \sim 32°$ and 74°, oscillating about the quasifree peak value for the other angles. Again, the $2D$ distribution cannot reproduce the experimental results. The distribution of the sum of $3S$ and $2D$ state contributions with proper normalization provide a fair fit to the shape of the experimental A_y vs T_p results. The greatest discrepancies are for the small proton angles (25° and 30°) and for proton energies on the extreme high and low energy ends of the spectra. The experimental distributions of the 25° and 30° data have a larger slope than that predicted by the DWIA calculation. It should be noted that the discrepancies are largest when the cross section is small. Thus, there could be contributions from other processes which do not have the same analyzing power as the one-step knockout reaction; for example, multistep processes which would be expected to produce a small analyzing power. The magnitude of the calculated analyzing-power distributions agrees very well with the experimental results for the $70°/-46.86°$ ($\theta_{c.m.} \sim 85°$) and $80°/-41.58°$ ($\theta_{c.m.} \sim 95°$) data. With the exception of the $90°/-36.55°$ angle pair, the other calculated analyzing powers are about 0.2 larger than the experimental result. This deviation is about the same as that at the quasifree peaks (see Fig. 2). If one artificially shifts the calculated spectra by 0.2, one would obtain an excellent agreement between calculation and experiment.

The same spectroscopic factors are used for the energy sharing cross section. The calculated results are plotted in Figs. 3—10 for the individual contributions and the sum. The $3S$ contribution alone gives a rather satisfactory fit to the experiment around the quasifree peaks, but underestimates the width of the distributions. The minimum predicted by a PWIA calculation for the $3S$ contribution around $p_3 \sim 150$ MeV/c is washed out further when a spin-orbit interaction is included in the distorting potential for $\theta_p \geq 40°$ while the opposite effect is observed for $\theta_p < 40°$. The $2D$ contribution is largest near $p_3 \sim 100$ MeV. The sum of $3S$ and $2D$ contributions gives a quite satisfactory fit to the energy-sharing spectra around the quasifree peak of all the data, but on the low T_p side of the spectra only for $\theta_p \geq 50°$. For $\theta_p \geq 50°$, the sum contribution of the $3S$ and $2D$ transition gives a half width at half maximum of $p_3 \approx 50$—55 MeV/c on the low T_p side which agrees with the experimental observation quite well. Any reasonable combination of these angular momenta could not reproduce the shape of the spectra on the low T_p side for $\theta_p \leq 40°$, even when the effects of the finite solid angle of the detector telescopes are taken into account. A similar difficulty also appears at the shoulders showing up on the high T_p side of $\theta_p \geq 60°$ spectra. These difficulties are encountered in other knockout reactions.[1,3,4] The discrepancies presumably arise from other

reaction processes such as the sequential alpha decay discussed previously, particularly for the high T_p side, and multistep processes when the cross sections are very small. In spite of these drawbacks, the agreement of the DWIA predictions with the energy-sharing spectra is generally encouraging.

V. CONCLUSIONS AND DISCUSSIONS

We have made measurements of $(\vec{p},p\alpha)$ on ^{9}Be for eight quasifree angle pairs ranging from $\theta_p=25°$ to 90° at $E_p=150.5$ MeV. Both analyzing powers and differential cross sections were obtained for energy-sharing distributions. The energy-sharing spectra show a prominent quasifree-knockout contribution, from which we obtain $L=0$ and 2 alpha spectroscopic factors of 0.45 and 0.55, respectively, in excellent agreement with previous experimental results and theoretical predictions. In general, the DWIA predictions fit the shapes of the energy-sharing spectra reasonably well. However, in addition to discrepancies due to sequential alpha-decay processes, there is a suggestion of a small yield due to multistep processes when the knockout cross section is small.

The angular distribution of the analyzing power at the quasifree peak is qualitatively in agreement with that of proton-alpha scattering at 147 MeV. The magnitudes of our results are somewhat lower, possibly suggesting a lower energy proton-alpha scattering. However, our results do agree with the new p+^{4}He data at 150 MeV. Irrespective of these slight differences, the experimental distribution is consistent with the p+^{4}He theoretical prediction and provides the first test of the quasifree cluster-knockout reaction theory using an intermediate energy polarized proton beam.

The shapes of the energy-sharing distributions of the experimental analyzing power agree fairly well with the theoretical prediction in the range of recoil momenta $|p_3|\leq 250$ MeV/c. This range includes $|p_3|\sim 150$ MeV/c where the PWIA fails completely. Our results provide evidence of the validity of the DWIA theory in this region. In addition, this distribution provides additional evidence for the D-state contribution and confirms the $L=2$ spectroscopic factor predicted by theory.

The inclusion of a spin-orbit term in the distorting potentials has negligible effect around the quasifree peak where the alpha-cluster momentum is small. However, at larger momenta on the low-proton-energy side for the S state the ratios of the differential cross sections with and without spin-orbit terms range from 0.35 at $\theta_p=25°$ to 1.7 at $\theta_p=70°$ decreasing to 1.3 at $\theta_p=90°$. For the D-state transition, the corresponding values are 0.8, 1.1, and 1.0. From the excellent agreement between theory and experiment shown in Figs. 6–10 on the low-proton-energy side, one can conclude that the inclusion of the spin-orbit effect in the DWIA calculation is necessary although it plays little role around the (p,pα) quasifree peak.

The average $L=0$ spectroscopic factor is in good agreement with previous experimental results and theoretical predictions. However, the values obtained from different angle pairs range from 0.36 to 0.61, a difference of about 70%. This difference is far beyond the experimental error. On referring to Eq. (1) of Sec. IV, it is evident that all factors are well defined except for the distorted-momentum-distribution amplitude and the half-off-shell two-body t operator. The effect of different distorting potentials on the distorted momentum distribution has been estimated to be 25% or less. Thus, it appears that the factorization of the half-off-shell t operator plays an important role in introducing this difference. A study covering a larger range of angles may help delineate this problem. However, it is beyond the scope of this paper.

Finally, from the present work it is clear that the DWIA theory contains the majority of the required reaction dynamics needed to describe (p,pα) reactions. Nevertheless, it underestimates the experimental yields on the low-proton-energy side of the energy-sharing spectra for $\theta_p\leq 40°$. It seems likely that these excessive yields are from reactions which are kinematically indistinguishable from the quasifree knockout. The analyzing-power data also suggests the need for an additional reaction mechanism with small analyzing power. If the mechanism in question is simply alpha decay following the inelastic excitation of the target nucleus, then kinematics require excitation energies in the range from 10 to 35 MeV.

ACKNOWLEDGMENTS

We are indebted to the Cyclotron staff of IUCF for their efforts in providing us with high quality and stable beams during the experimental work. This work was supported in part by the National Science Foundation. The work of C.W.W. was supported in part by the National Science Foundation and the Republic of China.

---

*On leave of absence from Institute of Physics, Academia Sinica, Taipei, Taiwan 115.

†Present address: Schlumberger Well Services-Engineering, Houston, TX 77210.

[1]T. A. Carey, P. G. Roos, N. S. Chant, A. Nadasen, and H. L. Chen, Phys. Rev. C **23**, 576 (1981); **29**, 1273 (1984).

[2]P. G. Roos, N. S. Chant, A. A. Cowley, D. A. Goldberg, H. D. Holmgren, and R. Woody III, Phys. Rev. C **15**, 69 (1977).

[3]N. S. Chant, in *Clustering Aspects of Nuclear Structure and Nuclear Reactions (Winnipeg, 1978)*, Proceedings of the Third International Conference on Clustering Aspects of Nuclear Structure and Nuclear Reactions, AIP Conf. Proc. No. 47, edited by W. T. H. van Oers, J. P. Svenne, J. S. C. McKee, and W. R. Falk (AIP, New York, 1978), p. 415, and references therein.

[4]A. Nadasen, N. S. Chant, P. G. Roos, T. A. Carey, R. Cowen, C. Samanta, and J. Wesick, Phys. Rev. C **22**, 1394 (1980).

[5]Joseph D. Sherman, D. L. Hendrie, and M. S. Zisman, Phys. Rev. C **13**, 20 (1976).

[6]C. W. Wang, N. S. Chant, P. G. Roos, A. Nadasen, T. Carey,

and A. A. Cowley, Phys. Rev. C **21**, 1705 (1980).
[7]C. Samanta, N. S. Chant, P. G. Roos, A. Nadasen, and A. A. Cowley, Phys. Rev. C **26**, 1379 (1982).
[8]F. D. Becchetti, in *Clustering Aspects of Nuclear Structure and Nuclear Reactions (Winnipeg, 1978)*, Proceedings of the Third International Conference on Clustering Aspects of Nuclear Structure and Nuclear Reactions, AIP Conf. Proc. No. 47, edited by W. T. H. van Oers, J. P. Svenne, J. S. C. McKee, and W. R. Falk (AIP, New York, 1978), p. 308, and references therein.
[9]G. J. Wozniak, D. P. Stahel, J. Cerny, and W. A. Jelley, Phys. Rev. C **14**, 815 (1976).
[10]N. Anantaraman, C. L. Bennett, J. P. Draayer, H. W. Fulbright, H. E. Gove, and J. Tōke, Phys. Rev. Lett. **35**, 1131 (1975).
[11]H. Yoshida, Phys. Lett. **47B**, 411 (1973).
[12]D. F. Jackson, Nucl. Phys. **A257**, 221 (1976).
[13]N. S. Chant and P. G. Roos, Phys. Rev. C **15**, 57 (1977).
[14]N. S. Chant and P. G. Roos, Phys. Rev. C **27**, 1060 (1983).
[15]A. A. Cowley, P. G. Roos, N. S. Chant, R. Woody III, H. D. Holmgren, and D. A. Goldberg, Phys. Rev. C **15**, 1650 (1977).
[16]J. L. Durand, J. Arvieux, C. Perrin, and G. Perrin, Phys. Lett. **53B**, 57 (1974).
[17]D. Kurath, Phys. Rev. C **7**, 1390 (1973).
[18]A. M. Cormack, J. N. Palmieri, N. F. Ramsey, and Richard Wilson, Phys. Rev. **115**, 599 (1959).
[19]J. S. Wesick, Ph.D. thesis, University of Maryland, 1983.
[20]P. G. Roos and N. S. Wall, Phys. Rev. **140**, B1237 (1965).